ISSN 1063-7826, Semiconductors, 2013, Vol. 47, No. 4, pp. 569–573. © Pleiades Publishing, Ltd., 2013.
Original Russian Text © I.A. Tambasov, V.G. Myagkov, A.A. Ivanenko, I.V. Nemtsev, L.E. Bykova, G.N. Bondarenko, J.L. Mihlin, I.A. Maksimov, V.V. Ivanov, S.V. Balashov, D.S. Karpenko, 2013, published in Fizika i Tekhnika Poluprovodnikov, 2013, Vol. 47, No. 4, pp. 546–550.

FABRICATION, TREATMENT, AND TESTING OF MATERIALS AND STRUCTURES

Structural and Optical Properties of Thin In_2O_3 Films Produced by Autowave Oxidation

I. A. Tambasov[a, c]^, V. G. Myagkov[a], A. A. Ivanenko[a], I. V. Nemtsev[a], L. E. Bykova[a], G. N. Bondarenko[b], J. L. Mihlin[b], I. A. Maksimov[b], V. V. Ivanov[c], S. V. Balashov[c], and D. S. Karpenko[c]

[a] *Kirenskii Institute of Physics, Siberian Branch, Russian Academy of Sciences, Krasnoyarsk, 660036 Russia*
^e-mail: tambasov_igor@mail.tu
[b] *Institute of Chemistry and Chemical Technology, Siberian Branch, Russian Academy of Sciences, Krasnoyarsk, 660049 Russia*
[c] *Joint Stock Company "Academician M.F. Reshetnev Information Satellite Systems", Zheleznogorsk, 662972 Russia*

Submitted May 16, 2012; accepted for publication May 31, 2012

Abstract—Cubic-phase In_2O_3 films are produced by the autowave oxidation reaction. Electron microscopy and photoelectron spectroscopy of the atomic profiles show that the samples are homogeneous over the entire area and throughout the thickness, with the typical grain size being 20–40 nm. The optical and electrical properties are studied for In_2O_3 films fabricated at different pressures in the vacuum chamber. In the wavelength range from 400 to 1100 nm, the transparency of the films was higher than 85%; the resistivity of the films was 1.8×10^{-2} Ω cm.

DOI: 10.1134/S1063782613040210

1. INTRODUCTION

At present, transparent conducting In_2O_3 thin films, both pure and doped with various impurities, are widely used for the production of gas sensors, thin-film transparent transistors, planar displays, electrochromatography devices, solar cells, etc. [1–4]. To date, different methods for the preparation of In_2O_3-based films have been developed. Among those are thermal vacuum deposition [1, 5, 6], magnetron-assisted sputtering [7, 8], pulsed laser deposition [9, 10], gas-phase deposition [11, 12], layer-by-layer atomic deposition [13], the sol–gel technique [14, 15], etc. In addition, there exist methods for the thermal vacuum deposition of pure indium with subsequent thermal oxidation at atmospheric pressure [16, 17]. However, these methods involve heating of the substrate to 500°C during deposition or subsequent annealing of the deposited films at temperatures of up to 70°C [18]. These conditions give rise to some difficulties in synthesizing indium-oxide films on thermally sensitive substrates. In addition, these production methods necessitate costly technological equipment and, when applied, present certain problems. Therefore, the development of low-temperature, inexpensive, simple methods for the production of In_2O_3 thin films is a topical problem.

In this study, we describe the synthesis of In_2O_3 thin films by the low-temperature autowave oxidation reaction in low vacuum (1.5–0.5 Torr). The results of studies of the structural, optical, and electrical characteristics of these films are reported.

2. EXPERIMENTAL

The initial In + In_2O_3 films were produced by thermal deposition of pure In onto glassy substrates in a vacuum chamber at a pressure of 1.5 Torr at room temperature. The glassy substrates were preliminarily cleaned [19]. The solid-phase reaction of oxidation of the initial In + In_2O_3 films was conducted by heating the substrate to 250°C at a rate of $\gtrsim 1$ K s^{-1} at pressures of 1.5, 0.9, and 0.5 Torr. Under such heating conditions, oxidation proceeded in the autowave reaction mode (as a combustion wave) at a rate of $v \approx 0.5$ cm s^{-1}. The autowave reaction mode consisted of the formation of an In_2O_3 nucleus spread throughout the entire film thickness and then the self-induced extension of the nucleus over the whole sample surface (Fig. 1).

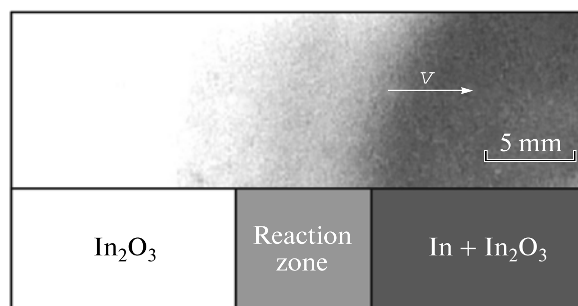

Fig. 1. Photograph (top) and schematic representation of autowave oxidation (bottom). Intensive oxidation processes occur at the reaction front only.

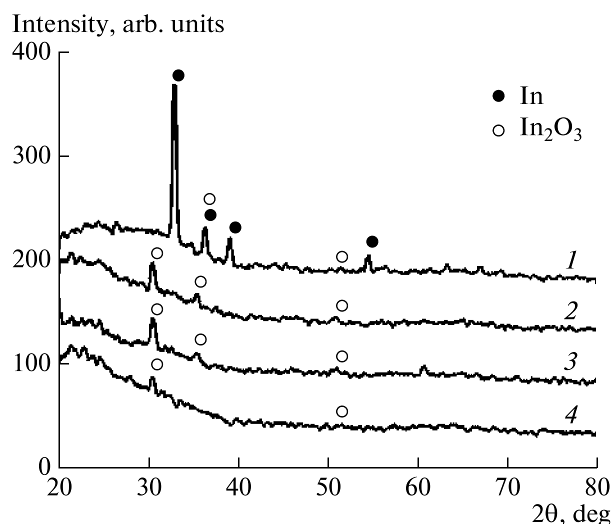

Fig. 2. X-ray diffraction patterns of the In_2O_3 films: (*1*) the initial sample and (*2–4*) the samples produced by autowave oxidation at vacuum-chamber pressures of (*2*) 1.5, (*3*) 0.9, and (*4*) 0.5 Torr.

However, at a heating rate lower than 1 k s^{-1}, the reaction proceeded over the whole film surface in the mode of slow reactive diffusion. For the first time, autowave oxidation of Co–Dy films was observed in [20, 21], where a possible mechanism for the autowave combustion mode was proposed. The autowave combustion mode in thin films is similar to self-propagating high-temperature synthesis (SPHTS) in powders, which is widely used for the production of new materials (see, e.g., [22–24]). It is thought that, compared to the initial mixture, SPHTS products contain smaller impurity fractions and are high-quality compounds [24]. However, the systematic features of reaction waves and the driving factors promoting their propagation in nanofilms remain poorly understood [25].

To determine the In_2O_3-film thicknesses, we used X-ray fluorescence analysis. The thicknesses were ~100–150 nm. The surface morphology of the In_2O_3 films was studied by scanning electron microscopy (SEM) with a Hitachi S5500 SEM microscope. X-ray diffraction (XRD) studies were carried out with a DRON-4-07 diffractometer (CuK_α radiation). The Scherrer formula was used to estimate the average grain size $d = 0.9\lambda/\Delta(2\theta)\cos\theta$, where λ, θ, and $\Delta(2\theta)$ are the wavelength, Bragg angles, and full width at half-maximum (FWHM) of the diffraction peak (in radians), respectively. The resistivity of the films was measured by the standard four-probe technique.

The chemical composition of the films was studied by X-ray photoelectron spectroscopy (XPS) using a SPECS GmbH spectrometer. The photoemission was excited by MgK_α radiation (1253.6 eV) emitted by an X-ray tube with a power of 180 W. The residual gas pressure in the analytical chamber was no higher than 1×10^{-9} mbar. The relative content of elements was determined from the survey spectra recorded at a transmission energy of 20 eV using a PHOIBOS 150 MCD9 semispherical energy analyzer, with the use of the empirical sensitivity coefficients. The spectra were calibrated in accordance with the binding energy C1*s* of the hydrocarbon contaminant layer (280.0 eV). To determine the profiles throughout the film thickness, we used sputtering with Ar^+ ions from a PU-IQE 12/38 ion gun directly in the analytical chamber. (The accelerating voltage and the ion current were, correspondingly, 2.5 kV and 15 μA, which provided an etching rate of 0.25–0.4 nm min^{-1}.)

The transmittance of the samples in the range 400–1100 nm was measured with a Bruker Vertex 80 spectrometer. All of the measurements were conducted at room temperature.

3. RESULTS AND DISCUSSION

Figure 2 shows the XRD pattern of the initial sample produced by the thermal evaporation of pure indium onto a glassy substrate. This XRD pattern shows the content of stable tetragonal (In) and cubic (In_2O_3) phases. The In_2O_3 phase is formed as a result of the partial oxidation of In under the conditions of In evaporation at a pressure of 1.5 Torr. However, the deposition rate of pure In is higher than the oxidation rate and the In_2O_3 deposition rate, resulting in the formation of In + In_2O_3 composite films. Analogous In + In_2O_3 composite films were produced previously by a similar technique [26, 27]. Figure 2 shows the XRD patterns of the In_2O_3 films produced in the autowave oxidation mode by heating of the initial In + In_2O_3 films to a temperature of 250°C at a rate higher than 1 K s^{-1} at different pressures in the vacuum chamber. For all of the films, the reaction initiation temperature was 180°C irrespective of the pressure in the vacuum chamber. After the reaction, all of the films contained the stable cubic In_2O_3 phase. A decrease in the peak height for the In_2O_3 phase is indicative of a decrease in grain size with decreasing pressure in the vacuum chamber (Fig. 2). Using the Scherrer formula, we estimated the average grain sizes to be ~25 nm for the initial In + In_2O_3 films and ~20 nm for the In_2O_3 samples produced by the autowave reaction at a pressure of 0.5 Torr.

Figure 3 shows the depth distributions of the In and O content in the initial In + In_2O_3 sample and in the sample after propagation of the oxidation wave at a vacuum-chamber pressure of 0.5 Torr. From the profiles shown in Fig. 3 and from the In 3*d* spectra, it can be seen that the initial films are not homogenous throughout the thickness and contain both metal In and indium oxide In_2O_3, which is predominantly due to oxidation of the film surface in contact with air. The In_2O_3 content is high also for the layers that are in con-

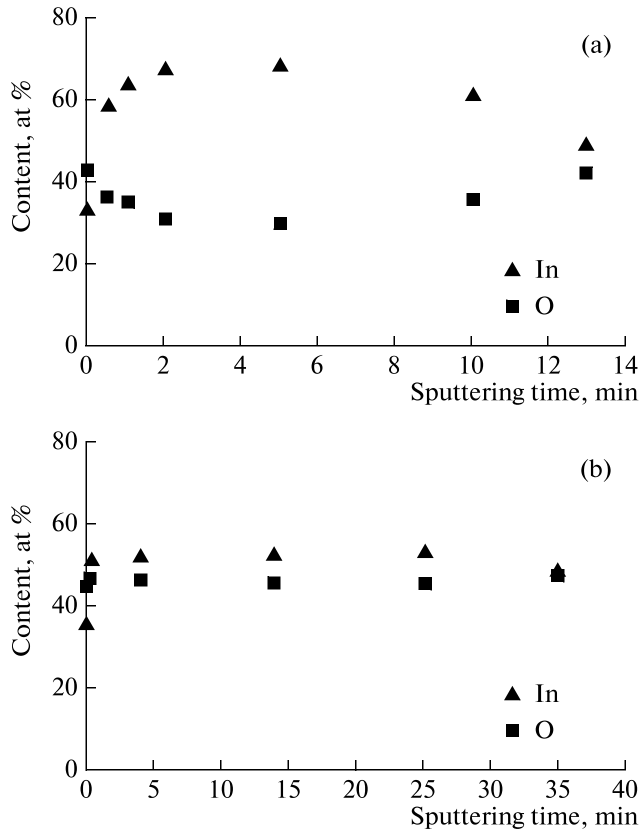

Fig. 3. Depth distribution of the In and O content in the initial In + In_2O_3 films (a) before and (b) after autowave oxidation at a pressure of 0.5 Torr.

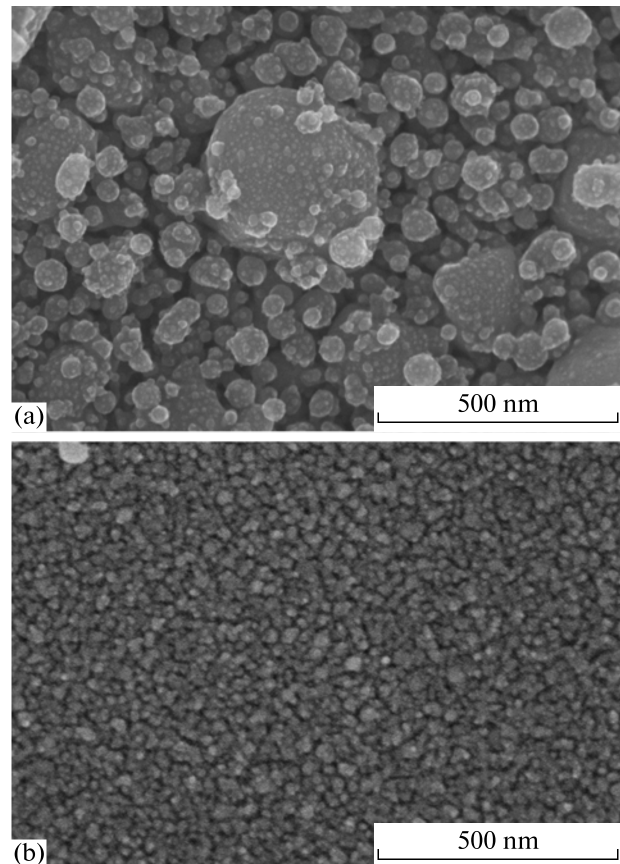

Fig. 4. SEM images of the surface of the initial In + In_2O_3 film (a) before and (b) after propagation of the oxidation wave at a pressure of 0.5 Torr.

tact with the substrate, and we also observe a line shifted to higher binding energies because of strong electrostatic recharging. In addition, indium oxide is also found within the film bulk. We think that this is due to the composite content of the initial In + In_2O_3 film formed with a variable In-deposition rate. After propagation of the oxidation wave over the film, the film components are intensively mixed, which makes the film homogeneous over the whole surface and throughout the thickness of the In_2O_3 film.

Figure 4 illustrates the surface morphology of the initial In + In_2O_3 sample and the sample after propagation of the oxidation wave at a pressure of 0.5 Torr. As can be seen from Fig. 4, the surface morphology of the as-deposited film before the reaction substantially differs from that of the film after the reaction. Before the reaction, the typical grain size is in a wide range from 30 to 400 nm. After propagation of the oxidation wave, the grain dimension is 20–40 nm and does not depend on the pressure in the vacuum chamber. Analysis of SEM microphotographs suggests that the surface of the In_2O_3 films synthesized by the autowave oxidation reaction is homogeneous. The grain sizes determined from the SEM data after the reaction are in good agreement with those determined from the XRD patterns by the Scherrer formula. However, for the initial In + In_2O_3 film, the Scherrer formula gives a size of 25 nm, which is an underestimate in comparison with the SEM average grain size. This is possibly due to the fact that the Scherrer formula does not take into account the wide size dispersion of grains (from 30 to 400 nm) in the initial samples.

Figure 5 shows the transmittance spectra of the In_2O_3 films produced by autowave oxidation of the initial In + In_2O_3 samples at pressures of 1.5, 0.9, and 0.5 Torr. All of the synthesized films exhibit high transmittance in the visible spectral region. From Fig. 5, it can be seen that there is a relationship between the transmittance and the pressure, at which the autowave oxidation reaction occurs. The transmittance decreases, as the pressure in the vacuum chamber, in which the oxidation reaction occurred, is elevated. To confirm the above inference, we fabricated an additional In_2O_3 sample at a pressure of 2.6 Torr (Fig. 5). The study of this sample supports the data on the decrease in the transmittance with increasing pressure during the reaction. However, if the pressure in the vacuum chamber is lowered to values below 0.5 Torr, the autowave oxidation reaction is not initiated. We think that,

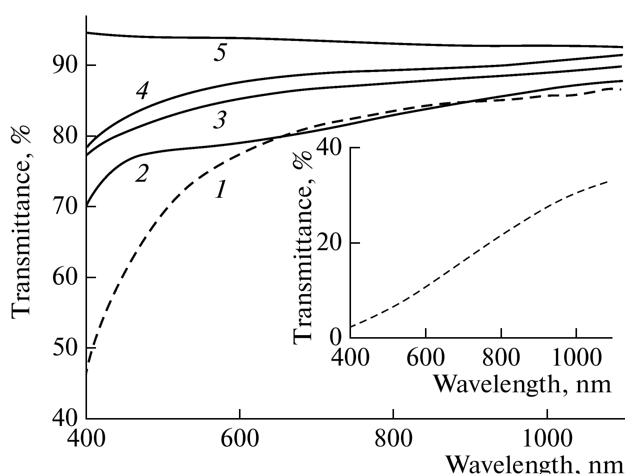

Fig. 5. Wavelength dependences of the transmittance of the In_2O_3 films produced by autowave oxidation at vacuum-chamber pressures of (*1*) 2.5, (*2*) 1.5, (*3*) 0.9, and (*4*) 0.5 Torr. Curve *5* shows the transmittance of the glassy substrate. The inset shows the transmittance of the initial ($In + In_2O_3$) film.

at pressures lower than 0.5 Torr, the oxygen content is inadequate to support the oxidation process. The maximum transmittance, 86%, is exhibited by the In_2O_3 films produced at a vacuum-chamber pressure of 0.5 Torr.

The resistivity of the synthesized In_2O_3 films unsteadily decreases, as the pressure in the vacuum chamber is lowered. The best characteristics are exhibited by the In_2O_3 films produced at a pressure of 0.5 Torr; the resistivity of such films is 1.8×10^{-2} Ω cm.

The table lists the values of the resistivity and transmittance for the In_2O_3 films produced by autowave oxidation at a pressure of 0.5 Torr here and by various techniques previously. From the table, it can be seen that, in their characteristics, the In_2O_3 films produced by autowave oxidation are comparable to those produced by other techniques. To the advantages of the autowave oxidation mode must be attributed the technological simplicity and the low temperature of In_2O_3-film synthesis.

From the thermal theories, it follows that the driving factor of combustion processes is the considerable heat release at the reaction front. Specifically, the main characteristics of the SPHTS processes is the high adiabatic temperature $T_{ad} \approx T_0 + Q/c$, where T_0 is the initial temperature, Q is the reaction heat with consideration for the phase transformation at the front, and c is the average heat capacity of the reaction products. To initiate the SPHTS reactions, it is essential that the adiabatic temperature T_{ad} be rather high; however, in most cases, the temperature T_{ad} does not exceed 5000 K [22–24]. The formation enthalpy and the average heat capacity of In_2O_3 are $\Delta H = -927$ kJ mol^{-1} and $c = 94$ J K^{-1} mol^{-1}, respectively [32]. Estimation of the adiabatic temperature of indium combustion in oxygen gives an extremely large value: $T_{ad} \approx 10000$ K. This temperature is much higher than that needed for the autowave reaction. However, in films, because of heat dissipation, the real temperature at the oxidation front is much lower than the adiabatic temperature.

From the results of this study, we can make an inference regarding the possible mechanism of the reaction. From Fig. 1, it follows that the reaction zone is ~0.5 cm in length. The reaction front propagating at a rate of $V \approx 0.5$ cm s^{-1} covers the above-indicated distance in a time of $t \approx 1$ s. In this time, in the reaction zone, oxygen diffuses throughout the film thickness $h \approx 100$ nm, which corresponds to the diffusion coefficient $D \approx h^2/t = 10^{-10}$ cm^2 c^{-1} for the solid phase. Since the reaction initiation temperature (180°C) is higher than the melting temperature of indium (121°C), oxygen initially diffuses into liquid indium with the formation of an In_2O_3 layer, whose melting temperature is high (1910°C). From the aforesaid, it follows that the In_2O_3 phase grows further due to oxygen diffusion throughout the In_2O_3 layer in the solid phase; i.e., the temperature of the oxidation front does not exceed the melting temperature of In_2O_3.

Comparison of the transmittances in the range 400–900 nm and the resistivities of In_2O_3 films

Transmittance, %	Resistivity, 10^{-2} Ω cm	Production technique	Reference
86.2	1.8	Autowave oxidation	This study
82.3	0.145	Gas-phase deposition at atmospheric pressure	[28]
73.3	0.17	Reactive electron-beam evaporation	[29]
73.2	10.6	Thermal oxidation of In films	[16]
86.7	0.027	Deposition by combined sputtering	[30]
88.6	4	Magnetron-assisted deposition	[8]
93.3	0.1	Activated reactive deposition	[31]
85	0.04	Pulsed laser deposition	[10]

4. CONCLUSIONS

A low-temperature technology for In_2O_3-film production is described. The technology is based on the thermal evaporation of pure indium in low vacuum (the residual pressure is no lower than 0.5 Torr) followed by heating to 250°C.

The process initiation temperature ($T_0 = 180°C$) and the heating rate (>1 K s^{-1}), above which the In_2O_3 films are synthesized in the autowave mode of the process at vacuum-chamber pressures of 1.5–0.5 Torr, are established.

It is shown that, after propagation of the oxidation wave, the layer of reaction products contains the cubic In_2O_3 phase uniformly distributed over the surface and throughout the thickness. In this phase, the typical grain size is 20–40 nm. The In_2O_3 films with the best characteristics are produced in vacuum, at a pressure of 0.5 Torr. The transmittance of the best films is higher than 85%, and the resistivity is 1.8×10^{-2} Ω cm.

REFERENCES

1. C. G. Granqvist, Solar Energy Mater. Solar Cells **91**, 1529 (2007).
2. S.-Y. Han, G. S. Herman, and Chin-hung Chang, J. Am. Chem. Soc. **133**, 5166 (2011).
3. R. E. Presley, C. L. Munsee, C.-H. Park, D. Hong, J. F. Wager, and D. A. Keszler, J. Phys. D: Appl. Phys. **37**, 2810 (2004).
4. A. A. Ivanenko, N. P. Shestakov, A. M. Sysoev, and V. F. Shabanov, in *Proceedings of the 7th World Multiconference on Systemics, Cybernetics, Informatics* (Orlando, 2003), vol. 10, p. 124.
5. K. D. Gopchandran, B. Joseph, J. T. Abraham, P. Koshy, and V. K. Vaidyan, Vacuum **48**, 547 (1997).
6. P. Koscielniak, J. Mazur, J. Henek, M. Kwoka, L. Pawela, and J. Szuber, Thin Solid Films **520**, 927 (2011).
7. S. I. Rembeza, P. E. Voronov, B. M. Sinel'nikov, and E. S. Rembeza, Semiconductors **45**, 1479 (2011).
8. S. Cho, Microelectron. Eng. **89**, 84 (2012).
9. D. A. Zuev, A. A. Lotin, O. A. Novodvorsky, F. V. Lebedev, O. D. Khramova, I. A. Petukhov, F. N. Putilin, A. N. Shatokhin, M. N. Rumyantseva, and A. M. Gas'kov, Semiconductors **46**, 410 (2012).
10. J. M. Dekkers, G. Rijnders, and H. A. Blank, Appl. Phys. Lett. **88**, 151908 (2006).
11. T. Maruyama and K. Fukui, Thin Solid Films **201**, 297 (1991).
12. A. Suzuki and K. Maki, Chem. Vapor Deposit. **12**, 608 (2006).
13. M. Ritala, T. Asikainen, and H. Leskela, Electronchem. Solid State Lett. **1**, 156 (1998).
14. R. B. H. Tahar, T. Ban, Y. Ohya, and Y. Takahashi, J. Appl. Phys. **83**, 2139 (1998).
15. C. Cantalini, W. Wlodarski, H. T. Sun, M. Z. Atashbar, M. Passacantando, A. R. Phani, and S. Santucci, Thin Solid Films **350**, 276 (1999).
16. V. D. Das, S. Kirupavathy, L. Damodare, and N. Lakshminarayan, J. Appl. Phys. **79**, 8521 (1996).
17. M. Girtan, G. I. Rusu, G. G. Rusu, and S. Gurlui, Appl. Surf. Sci. **162–163**, 492 (2000).
18. H. Kim, J. S. Horwitz, A. Pique, C. M. Gilmore, and D. B. Chrisey, Appl. Phys. A **69**, 447 (1999).
19. K. Ulutas, D. Deger, and Y. Skarlatos, Phys. Status Solidi A **203**, 2432 (2006).
20. V. G. Myagkov and V. S. Zhigalov, *Solid Phase Reactions and Phase Transformations in Layered Nanostructures* (Siberian Branch Acad. Sci., Novosibirsk, 2011) [in Russian].
21. V. G. Miagkov, L. I. Kveglis, G. I. Frolov, and V. S. Zhigalov, J. Mater. Sci. Lett. **13**, 1284 (1994).
22. A. G. Merzhanov, in *Physical Chemistry: Modern Problems*, Ed. by Ya. M. Kolotyrkin (Khimiya, Moscow, 1983) [in Russian].
23. A. G. Merzhanov, Russ. Chem. Rev. **72**, 289 (2003).
24. E. A. Levashov, A. S. Rogachev, V. I. Yukhvid, and I. P. Borovinskaya, *Physicochemical and Technological Bases of Self-Propagated High-Temperature Synthesis* (Binom, Moscow, 1999) [in Russian].
25. A. S. Rogachev, Russ. Chem. Rev. **77**, 21 (2008).
26. C. Kwon, J. Kim, H. J. Lee, H. C. Jung, and C. G. Park, J. Appl. Phys. **69**, 6716 (1991).
27. K. Ulutas, D. Deger, N. Kalkan, S. Yildirim, Y. G. Celebi, Y. Iskarlatos, M. L. Ovecogluz, and A. Genc, IOP Conf. Ser.: Mater. Sci. Eng. **15**, 012095 (2010).
28. D. W. Sheel and J. M. Gaskell, Thin Solid Films **520**, 1242 (2011).
29. I. Hamberg and C. G. Granqvist, J. Appl. Phys. **60**, R123 (1986).
30. M. Hest, M. S. Dabney, J. D. Perkins, and D. S. Ginley, Thin Solid Films **496**, 70 (2006).
31. P. Nath and R. F. Bunshah, Thin Solid Films **69**, 63 (1980).
32. *Short Manual of Physico-Chemical Valuers*, Ed. by K. P. Mishchenko and A. A. Ravdel (Khimiya, Leningrad, 1974) [in Russian].

Translated by E. Smorgonskaya